Two Step Synthesis and Application of Porous Carbon for Removal of Copper (II) from Wastewater: Statistical Optimization and Equilibrium Isotherm Analysis

Shobana Sinniha,[a] Zaira Zaman Chowdhury,[a,*] Ahmad Ibn Ibrahimy,[b] Mostak Ahmed,[a] Mohd. Rafie Bin Johan,[a] Mayeen Uddin Khandaker,[c] Irfan Anjum Badaruddin,[d] Sarfaraz Kamangar,[d] and Mohamed Hussien [e]

In this study, activated carbon (ACs) adsorbent was synthesized using the lignocellulosic waste (LCB) seed from *Adansonia digitata* L. (BSP) using two steps of hydrothermal carbonization (HTC) followed by activation. The hydrothermally produced char of BSP was activated to produce porous activated carbon BSPAC, where K_2CO_3 was used as a chemical activating agent. Box Behnken Design was used to optimize the input variables of pyrolysis temperature (A_1), residence time (B_1), and ratio (C_1) for the pyrolysis process. Removal percentage (β_1), percentage carbon yield (β_2), and fixed carbon (β_3) percentage were chosen as output responses. The analysis of variance was utilized to generate appropriate mathematical models with subsequent statistical analysis. Physiochemical characterizations were carried out for the hydrothermally carbonized sample (BSPC) and the optimized activated sample (BSPAC). Langmuir, Freundlich, and Temkin models were employed to estimate the isotherm model parameters. The results demonstrated that HTC with subsequent mild activation using K_2CO_3 can be considered as a greener route to obtain better-quality porous carbon having surface area of 599 m^2/gm for removal of Cu(II) cations from wastewater.

DOI: 10.15376/biores.19.2.3699-3724

Keywords: Hydrothermal carbonization; Adsorption; Box Behnken Design; Analysis of variance; Isotherm

*Contact information: a: Nanotechnology and Catalysis Research Center, University of Malaya, 50603 Malaysia; b: Department of Statistics and Finance, University of Malaya, 50603 Malaysia; c: Applied Physics and Radiation Technologies Group CCDCU, School of Engineering and Technology, Sunway University, Bandar Sunway, 47500 Selangor, Malaysia; Faculty of Graduate Studies, Daffodil International University, Daffodil Smart City, Birulia, Savar Dhaka, 1216, Bangladesh; d: Mechanical Engineering Department, College of Engineering, King Khalid University, Abha, 61421, Saudi Arabia; e: Department of Chemistry, King Khalid University, Abha, 61421, Saudi Arabia; *Corresponding author: dr.zaira.chowdhury@um.edu.my; Zaira.chowdhury76@gmail.com*

INTRODUCTION

The utilization of lignocellulosic waste (LCB) to generate sustainable bio-based products (carbon, bio-oil, and biogas) is essential for promoting the practice of a circular economy. LCB consists of three major types of biopolymers: cellulose, hemicellulose, and lignin. Porous activated carbons (ACs) produced from LCB can generate adsorbent materials to effectively remove copper(II) from wastewater. The transition metal of copper can exist as a zero valent copper (metal), monovalent cuprous ions-Cu(I), and divalent cupric ions-Cu(II). Due to their bioaccumulation tendency, divalent cations of Cu(II) may cause severe toxicity in living organisms (Ali *et al.* 2023). Copper is mainly used for

manufacturing semiconductors, electronic devices, and electro-plating processes. Long-term exposure to copper through polluted water can lead to diarrhea, nausea, and kidney and liver failures (Alcaraz *et al.* 2020; Mulungulungu *et al.* 2021). According to the EPA, USA, in drinking water, the copper level should not exceed to 1300 µ/L. Numerous approaches have been implemented to eliminate metallic pollutants from wastewater to comply with environmental regulations. There are several methods for treating wastewater, including electrochemical treatment (Ho *et al.* 2021), ion exchange (Virolainen *et al.* 2021), adsorption (Jin *et al.* 2018; Ali *et al.* 2023), and chemical precipitation (Tsai *et al.* 2020). In addition to its many advantages, adsorption is also recognized for its ease of implementation. Carbonaceous adsorbent can be regenerated and recycled after water treatment, which improves efficiency and reduces overall operating costs. Because of their substantial porous structure, large surface area containing functional groups, and resilience to harsh environmental conditions, carbon materials are widely used in water treatment (Chowdhury *et al.* 2016a; Adebisi *et al.* 2017). Regardless of extensive research carried out on developing new porous materials containing metal/organic frameworks (MOFs) (Rego *et al.* 2021) and covalent-organic frameworks (COFs) (Jiang *et al.* 2019) for the adsorptive removal of pollutants, such products are difficult to apply practically because of their high costs and complicated preparation methods. To address these obstacles, low-cost, effective, and sustainable carbonaceous materials must be developed from renewable sources of LCB residues (Chowdhury *et al.* 2012). Several biomass wastes, mainly containing lignocellulosic biopolymers (cellulose, hemicellulose, and lignin), have been used to produce activated carbon (ACs). Researchers have used physical, chemical, and physiochemical activation techniques to produce ACs from rice straw (Fierro *et al.* 2010), shell of palm and cocoa (Kundu *et al.* 2015; Saucier *et al.* 2015), frond of banana (Foo *et al.* 2013), peel of pomegranate and rambutan (Ahmad *et al.* 2014; Njoku *et al.* 2014), date stones (Abbas and Ahmed 2016), microalgae (Ferrera-Lorenzo *et al.* 2014), weeds of Crofton (Zheng *et al.* 2014), pulp mill sludge (Namazi *et al.* 2015), macadamia fruits' endocarp (Pezoti Junior *et al.* 2013), lignin waste (Maldhure and Ekhi 2011), corn stover (Zhu *et al.* 2015), *etc*.

Thermochemical conversion of LCB has gained attention from researchers because it can provide abundant, renewable feed stock, including biofuels, bioplastics, and carbonaceous materials, for versatile applications. The LCB is generated from forest and agricultural residues, solid organic matter from processing industries, wood, paper, and pulp. It is a carbon-neutral and renewable feedstock to produce useful chemicals (Adebisi *et al*. 2016). In general, LCB consists of 20% to 40% hemicellulose, 40% to 60% cellulose, and 10% to 24% lignin (Rajesh Banu *et al.* 2021). The global yearly production of LCB residues is around 181.5 billion tons, and approximately 8.2 billion tons are utilized for various applications (Singh *et al.* 2022). This illustrates the potential availability of LCB residues for conversion to yield a diverse spectrum of valuable chemical products. Transformation of LCB is paving avenues for its recycling and production of sustainable, eco-friendly products for energy, and environmental applications. It can be readily converted to value-added products using biochemical (microbial/enzymatic treatment) and thermochemical (pyrolysis, hydrothermal carbonization, gasification, combustion, and liquefication) conversion processes (Wang and Wu 2023; Singh *et al.* 2022). The processes of carbonization and pyrolysis are used to produce carbonaceous materials, biofuel, and syngas from LCB (cellulose, hemicellulose, and lignin) residues (Patel and Shah 2021). Careless disposal of this LCB waste can adversely affect the ecosystem by contaminating water and soil resources (Yu *et al.* 2021). It is possible to extend the

usefulness of LCB wastes even further through recycling and reprocessing. The potential of a material is not wasted but is further utilized rather than dumped.

Hydrothermal carbonization (HTC) is considered as one of the most efficient methods for carbonizing LCB to produce hydrochar, which can be converted to ACs for versatile applications. In this process, wet biomass is used, and energy-intensive pre-drying of biomass can be avoided (Benavente *et al.* 2015). Wet biomass is heated at relatively lower temperatures (120 to 350 °C) and under high pressure to obtain carbon-rich hydrochar. The characteristics of water change significantly under subcritical conditions. As the temperature increases from 100 to 350 °C, the pressure also increases, from 10 to 25 MPa. The dielectric constant of water decreases, and the strength of the hydrogen bonds also decreases in water. Water dissociates to form acidic hydronium ions (H_3O^+) and basic hydroxide (OH^-) ions. The degree of coalification is dependent on the temperature and time of the HTC process. Hydrochar contains different functional groups and can be converted to ACs with superior qualities to treat wastewater (Chowdhury *et al.* 2018).

In most of the literature, strong Lewis's acid-base catalysts of $ZnCl_2$, H_3PO_4, or KOH are used as activating agents. Application of these harsh, corrosive chemicals can induce secondary pollution in the environment. Based on the literature, there is a lack of research on the HTC of BSP to produce hydrochar (BSPC) and subsequently convert it into porous activated carbons (BSPAC) using K_2CO_3. The porous texture and surface-active sites of carbonaceous adsorbent can be tuned by optimizing the activation conditions, which can ensure sufficient removal of pollutant molecules from wastewater. Process input variables were optimized to obtain maximum output responses using Response Surface Methodology (RSM). Temperature (A_1), time (B_1), and impregnation ratio (C_1) were chosen as input variables using the Box Behnken Design (BBD). Three output responses/variables of percentage removal of copper, Cu(II) ions (β_1), percentage yield (β_2), and fixed carbon content (β_3) were estimated. Under optimum conditions, the hydrochar BSPC was activated. Resultant activated carbon of BSPAC was used to remove Cu(II) cations using the adsorption process. Thus, herein K_2CO_3 was used as a mild activating agent to produce superior-quality activated carbon (ACs). In this study, the adsorption performance of the optimum BSPAC sample was evaluated by estimating the equilibrium isotherm parameters. Linear regression analysis was completed for the adsorption data using Langmuir, Freundlich, and Temkin isotherm models. The findings of this study indicate that hydrochar-BSPC has the potential to serve as an effective substrate for the synthesis of porous activated carbons (BSPAC), which can be successfully utilized for the removal of Cu(II) ions from wastewater.

EXPERIMENTAL

Materials

Adansonia digitata L. (baobab) seed was collected from Malaysian Agricultural Research and Development (MARDI). It was crushed to powder and washed with deionized water (DI). It was then dried at 60 °C for 24 h and stored in an airtight container. Potassium carbonate (K_2CO_3) was obtained from Sigma Aldrich, Malaysia. Analytical grade copper sulphate penta hydrate ($CuSO_4 \cdot 5H_2O$) salt, HCl, and NaOH were obtained from Merck, Malaysia.

Methodology

Hydrothermal carbonization of Baobab seed powder (BSP)

The hydrochar was prepared from the washed and dried baobab seed powder (BSP). HTC was carried out in inert atmosphere by passing N_2 gas to prevent sample burning and deionized water (DI) was used as solvent. About 10 g of BSP biomass sample was mixed with 100 mL DI water and placed inside the Teflon-lined autoclave. The temperature was kept at 180 °C for 120 min. The synthesized hydrochar was labelled as BSPC, washed with DI water until the pH reached 7, and dried under vacuum oven overnight at 50 °C. The BSPC sample was refluxed with preselected weight of K_2CO_3 based on Box Behnken Design (BBD) as provided by Tables 1 and 2. The samples of hydrochar were refluxed for 6 h at 60 °C. It was then filtered to remove excess K_2CO_3. The samples were washed vigorously. It was dried in vacuum oven to prevent burning at 50 °C overnight. The samples were stored for activation under different experimental conditions of temperature (A_1) and time (B_1) as shown by the design matrix of Tables 1 and 2.

Fixed bed pyrolysis to produce activated carbon BSPAC from hydrochar BSPC

Approximately 40 g of K_2CO_3 impregnated hydro-char (BSPC) was placed inside the fixed bed reactor and N_2 gas flow was given at 100 mL/min to ensure inert atmosphere and then the gas cylinder was changed to CO_2 gas flow. The gas flow rate for CO_2 was maintained at 100 mL/min. The temperature and time were changed according to the design matrix provided by Tables 1 and 2. The N_2 gas flow was changed to CO_2 gas flow after the reactor reached a stable temperature as suggested by the design matrix of Table 2. Thus, the activation of hydrochar was carried out for specific temperature (A_1) and duration (B_1) after refluxing them with predetermined ratio of K_2CO_3 (C_1) (Table 2). The synthesized ACs from 17 experimental runs (Table 2) were meticulously washed using hot DI water to eliminate the remaining chemical solution until the pH reached 7. The samples were dried under vacuum oven at 50 °C overnight. The samples were stored for further characterizations and the results obtained were tabulated in Table 2 for development of regression model, ANOVA analysis, and process optimization using numerical approach. Tables 1 and 2 illustrate the RSM-BBD design layout for activation conditions.

Table 1. Input/Independent Variables using Box Behnken Design for Activation of hydrochar BSPC

Input Factors/Variables	Code	Coded Levels			Output Responses/Variable
		-1	0	+1	
Temperature (°C)	A_1	500	650	800	Removal Percentages (β_1) Percentage Yield (β_2) Percentage Fixed Carbon content (β_3)
Activation Time (h)	B_1	1	0.5	2	
K_2CO_3 Weight Ratio (w/w)	C_1	0.5	1	2	

The experimental run number (N) required for three input variables can be expressed by Eq. 1,

$$N = 2k\,(k - 1) + C_0 \quad (1)$$

where k signifies the number of variables, C_0 shows the number of central points, and where under same conditions, experiments are repeated.

Table 2. Box-Behnken Factorial Design for Preparation of BSPAC from BSPC

Sample No	Run No	Point Type	Input Variables for Activation			Cu(II) Removal (%)	Yield (%)	Fixed Carbon Content (%)
			Temp A_1 (°C)	Time B_1 (h)	Ratio C_1 (w/w)	β_1	β_2	β_3
13	1	Center	650.00	1.5	1.25	70.99	88.78	71.23
14	2	Center	650.00	1.5	1.25	70.65	88.54	71.33
15	4	Center	650.00	1.5	1.25	71.32	87.99	70.99
16	6	Center	650.00	1.5	1.25	71.89	88.43	71.43
17	13	Center	650.00	1.5	1.25	70.49	88.56	71.34
1	3	IBFact	800.00	1.5	2.00	90.76	78.56	82.66
2	5	IBFact	500.00	1.5	0.50	61.97	92.94	67.55
3	7	IBFact	500.00	2.0	1.25	69.66	89.55	70.89
4	8	IBFact	500.00	1.0	1.25	62.21	90.06	64.88
5	9	IBFact	650.00	1.0	0.50	58.87	87.45	66.77
6	10	IBFact	800.00	1.0	1.25	82.32	80.18	77.99
7	11	IBFact	800.00	2.0	1.25	90.94	71.55	81.55
8	12	IBFact	650.00	2.0	2.00	78.88	84.66	82.54
9	14	IBFact	800.00	1.5	0.50	80.76	78.19	77.55
10	15	IBFact	650.00	1.0	2.00	69.87	88.44	70.54
11	16	IBFact	500.00	1.5	2.00	70.65	88.87	71.88
12	17	IBFact	650.00	2.0	0.50	69.45	86.09	76.21

In this study, three input variables of activation temperature (A_1), residence time (B_1), and weight ratio (C_1) between hydrochar (BSPC) and activating agent of K_2CO_3 were chosen. The desired responses/output variables were percentages removal of Cu(II) from wastewater (β_1), yield percentages (β_2), and fixed carbon content (β_3). The lower, middle, and higher levels of each factor/variable were indicated as -1, 0, and +1, correspondingly (Adebesi *et al.* 2016; Pei *et al.* 2023). The experimental runs can be randomized, and the second order regression model can be expressed using the Eq. 2 (Chowdhury *et al.* 2016b; Ayed *et al.* 2019;),

$$Y = b_0 + \sum_{i=1}^{n} b_1 x_1 + \sum_{i=1}^{n} b_{11} x_i^2 + \sum_{i=1}^{n} \sum_{j>1}^{n} b_{ij} x_i x_j \quad (2)$$

where Y is the preselected response, constant coefficient is b_0, the linear coefficient is b_i, b_{ij} denotes the interaction coefficients, b_{ii} is the coefficient for quadratic terms. Here, x_i and x_j reflect the coded values of variables (Chowdhury *et al.* 2016b;). Five trials are needed at the center point for the three input variables, and overall, 17 experiments (N) are required (Table 2) (Adebesi *et al.* 2016; Pei *et al.* 2023).

Equilibrium adsorption studies

A precise amount of BSPAC sample prepared under optimum condition was placed inside the plastic bottles containing the adsorbate - Cu(II) solution, where the concentration ranges were varied from 50 to 100 mg/L. The samples were agitated at 250 rpm. To ensure true adsorption rather than precipitation, the pH was kept constant at pH 5.5. Removal percentages of Cu(II) cations were estimated using Eq. 3 and yield percentages were determined by Eq. 4:

$$Removal\ Percentages\ (\beta_1) = \frac{C_0 - C_e}{C_0} \times 100 \quad (3)$$

$$Activated\ Carbon\ Yield\ (\beta_2) = \frac{Initial\ weight\ of\ Hydrochar\ (g) - Final\ weight\ of\ Activated\ Carbon\ (g)}{Initial\ weight\ of\ Hydrochar\ (g)} x100 \quad (4)$$

Equations 5 and 6 were used to calculate amount of adsorbate (Cu(II) cations) ions, q_t (mg/g) at different time t and q_e (mg/g) after equilibrium contact time, t (min) (Adebesi *et al.* 2017a). Equations 5 and 6 are as follows,

Amount of Adsorbate over solid surface at equilibrium time, $q_e = \frac{(C_0 - C_e)V}{W}$ (5)

Amount of Adsorbate over solid surface at specific interval time, $q_t = \frac{(C_0 - C_t)V}{W}$ (6)

where C_0 is the initial concentration of the pollutant adsorbate of Cu(II) cations, C_e is the remaining equilibrium concentration in liquid phase; both in mg/L, W is the weight of adsorbent carbon in g and volume of adsorbate solution is V in L (Akinpelu *et al.* 2021;).

The adsorption isotherm serves to establish a correlation between the concentration of a pollutant or adsorbate in a liquid medium and its adsorbed amount onto the solid adsorbent surface. Linear regression analyses for Langmuir, Freundlich, and Temkin isotherms were run. The suitability of the model was checked by estimating the values of R^2 along with some model constants. An adsorption system is better represented by a model; with an R^2 value near to unity (Adebesi *et al.* 2017b; Huang and Garcia-Bennett 2021).

According to the Langmuir adsorption isotherm, changes in pressure inside the equilibrium system affect the amounts of pollutants adsorbed. The observation illustrates the correlation between the number of active sites over the adsorbent and the pressure. A monolayer of pollutant can accumulate over the homogeneous surface of adsorbent (Doan *et al.* 2021; Mittal *et al.* 2021;). However, it should be noted that the Langmuir isotherm is applicable specifically at lower temperatures. Langmuir adsorption model can be represented by Eqs. 7, 8, and 9,

$$q_e = \frac{q_{max} K_L C_e}{1+K_L C_e} \quad (7)$$

$$\frac{C_e}{q_e} = \frac{1}{q_{max} K_L} + \frac{1}{q_{max}} C_e \quad (8)$$

$$R_L = \frac{1}{1+K_L C_0} \quad (9)$$

where equilibrium adsorbed amount is denoted by q_e (mg/g), q_m (mg/g) is the maximum monolayer adsorption capacity, C_e represents the concentration of the pollutant at equilibrium, and the energy of adsorption is defined by Langmuir adsorption constant K_L. If Langmuir constant R_L = 1; the process is linear, for R_L> 1, the process is unfavourable; R_L= 0, the process is irreversible, and for 0 < R_L< 1, the process is favourable.

According to Freundlich isotherms, pollutants can form multilayer over the heterogeneous surface of the adsorbents (Akinpelu *et al.* 2021). The linear and nonlinear forms of Freundlich isotherms are given as Eqs. 10 and 11: $q_e = K_f C_e^{1/n}$ (10)

$$Ln\, q_e = LnK_f + \frac{1}{n} Ln\, C_e \quad (11)$$

Here, $1/n$ reflects sorption affinity and K_F (mg/g) (L/mg)$^{1/n}$ denotes constant for Freundlich isotherm. Freundlich isotherm states that sorption is linear at low pressure but independent at high pressure.

The Temkin isotherm suggests a progressive decrease in the heat of sorption with increasing surface coverage. Additionally, during the sorption process, there are indirect interactions between the adsorbate and adsorbent (Chowdhury *et al.* 2015; Akinpelu *et al.* 2021). Linear and non-linear equations of Temkin model are:

$$q_e = \frac{RT}{b} LnK_T C_e \quad (12)$$

$$q_e = \frac{RT}{b} Ln\, K_T + \frac{RT}{b} \quad (13)$$

where Temkin constant is $B = RT/b$, which correlates with the heat of sorption, and the Binding constant is K_T (L/g). Solution absolute temperature is T (°K), and universal constant is R = 8.314 J/mol.K).

Characterizations

The surface morphological features showing texture of surface along with pore characteristics of starting biomass (BSP), hydrochar (BSPC), and their respective activated carbon (BSPAC) prepared under optimum conditions were observed using field emission scanning electron microscopy (FESEM- Fei Quanta Feg-450, Malaysia). Thermogravimetric/proximate analysis (TGA) of BSP, BSPC, and BSPAC were performed using an analyzer (TGA-Mettler Toledo TGA/SDTA 851e, USA). This would estimate the percentage fixed carbon, volatile materials, moisture, as well as ash proportion of the sample. The temperature was raised from 30 ℃ to 850 ℃ under air and nitrogen flow to calculate the weight loss of the samples in each stage. Elemental analyzer was used in (PerkinElmer- Series II 2400, Japan) to calculate the proportion of carbon, hydrogen, nitrogen, and others in the starting BSP, hydrochar (BSPC), and activated carbon (BSPAC) samples. Nitrogen gas adsorption-desorption analysis was carried out at 77 °K to measure the surface area, pore diameter, and pore volume of the synthesized samples. The synthesized samples were outgassed before Brunauer Emmett Teller (BET) analysis for 4

h at 300 °C. After that, BET analysis (Tri-Star II Micrometrics surface area analyzer, USA) was carried out to analyze the pore size distribution of BSPC and BSPAC samples.

RESULTS AND DISCUSSION

Fitting of Regression Model and Statistical Analysis for Activation of Hydrochar (BSPC) to Produce Activated Carbon (BSPAC)

Regression models were developed for three responses of removal percentages of Cu(II) cations (β_1), yield percentages (β_2), and fixed carbon content (β_3) percentages. The developed models were formulated using the highest degree of polynomial equations for all three responses, which included significant additional terms. Based on the sequential model sum of squares, it was determined that these models were not aliased. Quadratic models were proposed for copper removal percentages (β_1) and yield percentages (β_2). A linear model was suggested for fixed carbon content percentages (β_3). The underlying empirical equations proposed by BBD design are represented by Eqs. 14, 15, and 16 as a function of coded variables after deleting unnecessary factors from the responses. The reliability of the designs can be verified by examining the plots of experimental *versus* predicted data points and can be represented by Figs. 1(a), 1(b), and 1(c).

$$Removal\ Percentages\ of\ Copper, Cu(II) Cations\ (\beta_1) = +71.07 + 10.04A_1 + 4.46\ B_1 + 4.89C_1 + 0.29A_1B_1 + 0.33A_1C_1 - 0.39B_1C_1 + 5.99A_1^2 - 0.78B_1^2 - 1.06\ C_1^2 \quad (14)$$

$$Carbon\ Yield\ Percentages\ (\beta_2) = +88.46 - 6.62\ A_1 - 1.79B_1 - 0.52C_1 - 2.03\ A_1B_1 + 1.11A_1C_1 - 0.61\ B_1C_1 - 3.82A_1^2 - 1.80\ B_1^2 + 0.025\ C_1^2 \quad (15)$$

$$Fixed\ Carbon\ Percentages\ (\beta_3) = +73.03 + 5.57A_1 + 3.88B_1 + 2.44C_1 \quad (16)$$

For a single parameter of pyrolysis temperature (A_1), time (B_1), and ratio (C_1), the coefficient was derived based on the contribution of that specific factor in determining the removal percentage (β_1), carbon yield (β_2), and fixed carbon content (β_3). The second-order terms reflected the quadratic impact of that variable. For all the above equations of 14, 15, and 16; positive sign preceding the term implied a synergistic relationship, whereas the negative sign reflected an antagonistic impact (Chowdhury *et al.* 2012; Ayed *et al.* 2019). To assess the reliability of the developed model, the coefficient of determination, R^2, and standard deviation (SD%) values should be analyzed. The R^2 values statistically indicate how accurately a model correlates with the experimental data (Adebesi *et al.* 2016). The R^2 values for Eqs. 14, 15, and 16 were 0.997, 0.990, and 0.881, respectively. The multiplication of coefficients of two variables confirmed the cumulative effect of two factors/variables.

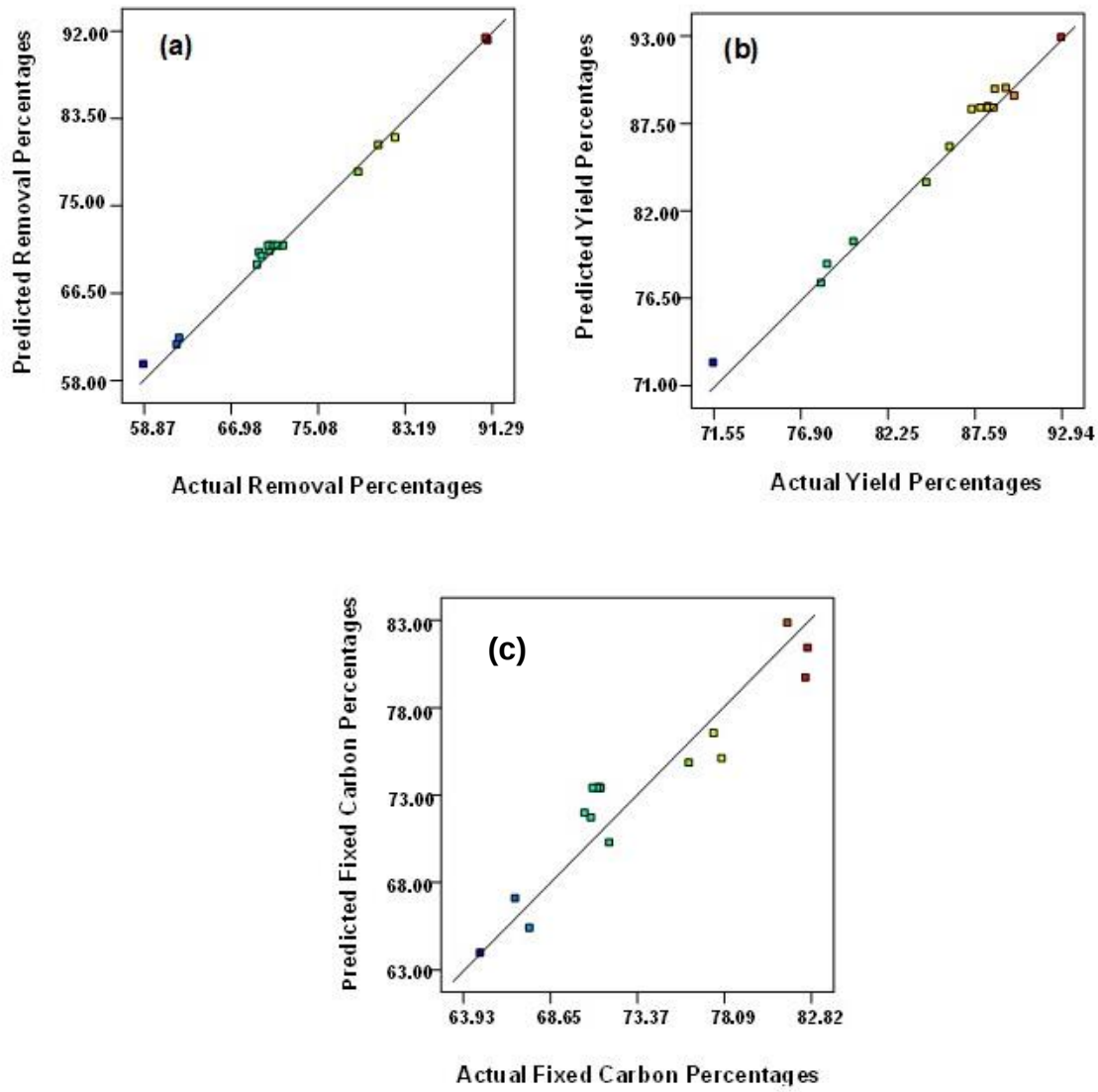

Fig. 1. Actual/experimental versus predicted data points (a); percentage removal β_1 (b); percentage yield β_2 (c); and percentage fixed carbon β_3 for BSPAC

The results obtained from ANOVA analysis are presented in Tables 3, 4, and 5 for removal percentages (β_1), yield percentages (β_2), and fixed carbon content percentages (β_3), respectively. The F-values obtained here for removal percentages of Cu(II) cations (β_1), percentage yield (β_2), and percentage fixed carbon content (β_3) were 257.58, 80.01, and 31.99, respectively. This reflects that the models developed here, were significant. The Prob > F values were below 0.05, suggesting that the model input variables chosen for the specified responses held statistical significance (Chowdhury *et al.* 2012).

Table 3. ANOVA and Statistical Analysis for Effect of Input Parameters/Variables on Percentage Removal (β_1)

Source	Sum of Squares	Degree of Freedom	Mean Square	F Value	Prob> F	Comments
Model	1311.66	9	145.47	257.58	<0.0001	*Significant*
A_1	805.81	1	805.81	1424.1	<0.0001	
B_1	158.95	1	158.95	280.13	<0.0001	
C_1	191.20	1	191.20	337.92	<0.0001	
A_1B_1	0.34	1	0.34	0.60	0.4622	
A_1C_1	0.44	1	0.44	0.77	0.4094	
B_1C_1	0.62	1	0.62	1.09	0.3314	
A_1^2	151.12	1	151.12	267.09	<0.0001	
B_1^2	2.54	1	2.54	4.49	0.0719	
C_1^2	4.42	1	4.42	7.80	0.0268	
Residuals	3.96	7	0.57			
Lack of Fit	2.71	3	0.90	2.88	0.1668	
Pure Error	1.25	4	0.31			
Statistical Tools						
Standard Deviation SD%						0.75
Mean						73.04
Correlation Coefficient, R^2						0.997
Adjusted R^2						0.993
Predicted R^2						0.965
Coefficient of Variation, CV						1.03
Adequate Precision						55.03

The variables of temperature (A_1), residence time (B_1), ratio (C_1), and their quadratic terms A_1^2 and C_1^2 were significant for the percentage removal, β_1. Compared to temperature (A_1), other linear variables of time (B_1), and ratio (C_1) had moderate effect on the percentage removal (β_1). The interaction between temperature and time (A_1B_1) had greater impact on the responses of percentage removal, β_1, than the other interaction variables of B_1C_1 and C_1A_1(Table 3).

For yield percentages (β_2), linear terms of temperature (A_1), time (B_1), their interaction terms A_1B_1 and $A_1C_1$and their quadratic terms A_1^2, and B_1^2 were significant. Temperature had the greatest influence on this response. The interaction between time and ratio (B_1C_1) had more prominent influence rather than the other interaction terms ($C_1A_1$and A_1B_1) on percentage yield, β_2 (Table 4). For fixed carbon content percentages, β_3; temperature (A_1), time (B_1), and ratio (C_1) were significant model terms (Table 5). The obtained standard deviations (SD%) and coefficient of variation (CV) were minimal, implying that the suggested models are dependable (Tables 3, 4, and 5) (Sellamuthu *et al.* 2023). The signal/noise ratio (*s*/*n*) achieved in this case exceeded 4, indicating sufficient precision for the proposed models (Sellamuthu *et al.* 2023). The adequate precision values obtained for removal percentages for β_1, percentage yield β_2, and fixed carbon content β_3,

were 55.03, 19.74, and 18.70, respectively. Therefore, the experimental data collected in this research held statistical importance for directing the design (Sellamuthu *et al*. 2023).

Table 4. ANOVA and Statistical Analysis for Effect of Input Parameters/Variables on Percentage Yield (β_2)

Source	Sum of Squares	Degree of Freedom	Mean Square	F Value	Prob> F	Comments
Model	479.72	9	53.30	80.01	<0.0001	*Significant*
A_1	350.33	1	350.33	525.90	<0.0001	
B_1	25.49	1	25.49	38.26	0.0005	
C_1	2.14	1	2.14	3.22	0.1160	
A_1B_1	16.48	1	16.48	24.74	0.0016	
A_1C_1	4.93	1	4.93	7.40	0.0298	
B_1C_1	1.46	1	1.46	2.20	0.1818	
A_1^2	61.52	1	61.52	92.35	<0.0001	
B_1^2	13.68	1	13.68	20.54	0.0027	
C_1^2	0.0263	1	0.0263	0.0039	0.9954	
Residuals	4.66	7	1.02			
Lack of Fit	4.32	3	2.28	16.92	0.0092	
Pure Error	0.34	4	0.08			
Statistical Tools						
Standard Deviation SD%						0.82
Mean						85.81
Correlation Coefficient, R^2						0.990
Adjusted R^2						0.971
Predicted R^2						0.856
Coefficient of Variation, CV						0.95
Adequate Precision						19.74

The impact of processing variables on percentage removal (β_1)

According to the F values reported in Table 3, it was concluded that the pyrolysis temperature (A_1) had the strongest influence on percentage removal (β_1), and the duration (B_1) and ratio (C_1) had approximately lower effects on this response. When the ratio was adjusted at center/zero, the trend for sorption capacity was quantified and the combined impact of temperature (A_1) and time (B_1) was illustrated by 3D RSM mesh plot of Fig. 2(a). A schematic representation of the impact of ratio (C_1) and time (B_1) on the removal percentages (β_1) is presented in Fig. 2(b), in which the temperature (A_1) was maintained constant at zero level.

A lot of studies have shown that activation time, as well as temperature, can diminish the surface area and sorption capacity of the synthesized ACs if the limit of those two factors is extremely high or low. A prolonged pyrolysis time or excessive pyrolysis temperature could adversely affect the existing porous structure (Chowdhury *et al*. 2016c).

Similarly, insufficient activation time and/or a reduced temperature of activation cannot improve the porosities of the carbonaceous adsorbent. Thus, process optimization is needed to maintain the quality of the carbon (Sellamuthu *et al.* 2023).

Table 5. ANOVA and Statistical Analysis for Effect of Input Parameters/Variables on Percentage Fixed Carbon (β_3)

Source	Sum of Squares	Degree of Freedom	Mean Square	F Value	Prob> F	Comments
Model	416.02	3	138.67	31.99	<0.0001	*Significant*
A_1	248.09	1	248.09	37.23	<0.0001	
B_1	120.20	1	120.20	27.73	<0.0002	
C_1	47.33	1	47.33	11.01	0.0056	
Residuals	56.35	13	4.33			
Lack of Fit	56.24	9	6.25	219.41	<0.0001	
Pure Error	0.11	4	0.028			
Statistical Tools						
Standard Deviation SD%						2.08
Mean						73.37
Correlation Coefficient, R^2						0.881
Adjusted R^2						0.853
Predicted R^2						0.791
Coefficient of Variation, CV						2.08
Adequate Precision						18.70

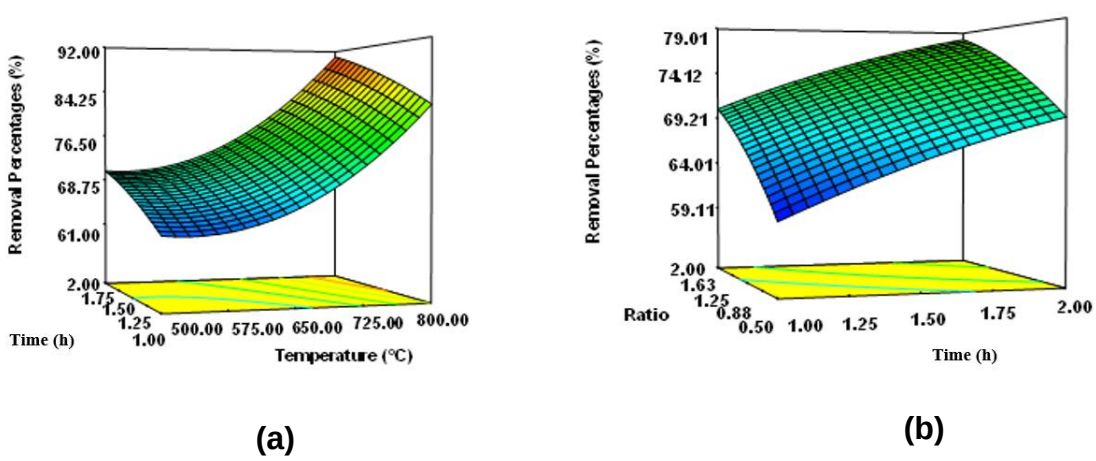

Fig. 2. 3D Response surface plots for percentage removal (β_1): (a) influence of temperature (A_1) and time (B_1) when ratio (C_1) was constant at zero/center points (1.25); (b) Influence of time (B_1) and ratio (C_1) when temperature (A_1) was constant at zero/center points (650 °C)

The higher the temperature, the more likely it is that micropores walls will deform and eventually break, to form mesopores. This will facilitate the penetration of the pollutant

adsorbate inside the porous region of the carbon matrix. Even with an extensive surface area, if the size of mesopores is excessively large, it will be ineffective in capturing and retaining the smaller metallic cations. This leads to a decrease in removal efficiency (Chowdhury *et al.* 2017).

A synergistic relationship between the three variables and the removal efficiencies (β_1**)** was observed in this study. Gradually raising the temperature and allowing sufficient contact time for activation would increase the reaction rate between the hydrochar and K_2CO_3. Thus, high-quality ACs can be produced by increasing the activation time and temperature up to a certain level. Beyond that certain limit, the ACs samples will deteriorate.

It can be observed from Fig. 2(a) that, the removal percentages decreased slightly after exceeding the specific limit of time and temperature. With increasing K_2CO_3 ratio, as well as time, the removal percentages were increasing (Fig. 2b). In some cases, excessive temperature may result in degradation of certain functional groups as well as porous texture of carbon, leading to more ash formation. Although the impregnation ratio was important in the development of pores, it was not the only factor. The increase in K_2CO_3 enhanced the reaction rate, resulting in an increase in the number of pores in the carbon. High concentration of K_2CO_3 was not also favourable. In that case, additional chemical reactions between K_2CO_3 and hydrochar can cause the destruction of pores that had existed previously. This might reduce the amount of fixed carbon content and increase the formation of ash residues.

The impact of processing variables on percentage yield (β_2)

The impact of process variables on activated carbon yield (β_2) was demonstrated by 3D response surfaces plots, presented by Figs. 3(a and b).

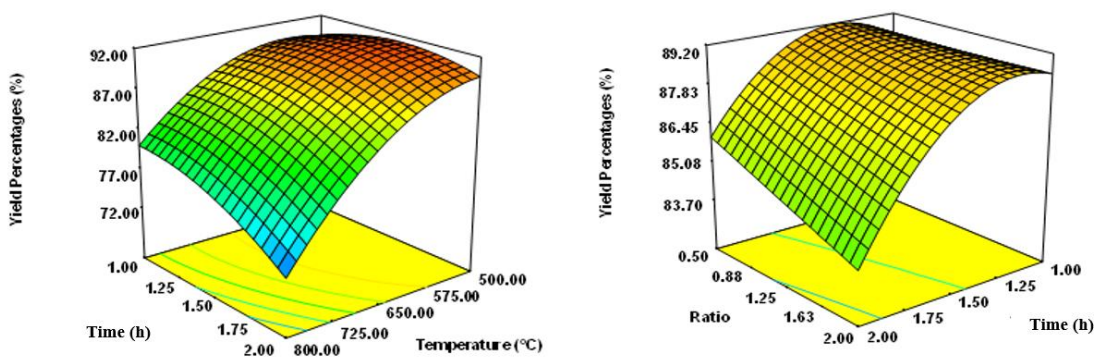

(a) **(b)**

Fig. 3. 3D Response surface plots for percentage yield (β_2): (a) influence of temperature (A_1) and time (B_1) when ratio (C_1) was constant at zero/center points (1.25); (b) influence of time (B_1) and ratio (C_1) when temperature (A_1) was constant at zero/center points (650 °C)

Figure 3(a) represents the overall impact of temperature (A_1) and pyrolysis time (B_1) on yield percentages (β_2) where the ratio (C_1) between hydrochar (BSPC) and K_2CO_3 was kept at zero level (ratio = 1.25). The influence of pyrolysis time (B_1) and impregnation ratio (C_1) on activated carbon yield (β_2) percentages are shown by Fig. 3(b), where the temperature was kept at zero level (650 °C). In general, it was discovered that the yield of

carbon (β_2) decreased with increasing reaction temperature (A_1), time (B_1), and ratio (C_1). As observed from Figs. 3a and b, the temperature had a greater influence on the carbon yield. Carbon yield was minimum when the sample was pyrolyzed at temperature 800 °C for 2 h and the ratio was 1.25. In contrast, the impact of activation time on the yield percentages was moderate. A rise in temperature would increase volatile compound discharge due to increased dehydration and elimination processes during the activation. It would finally decrease the yield of BSPAC.

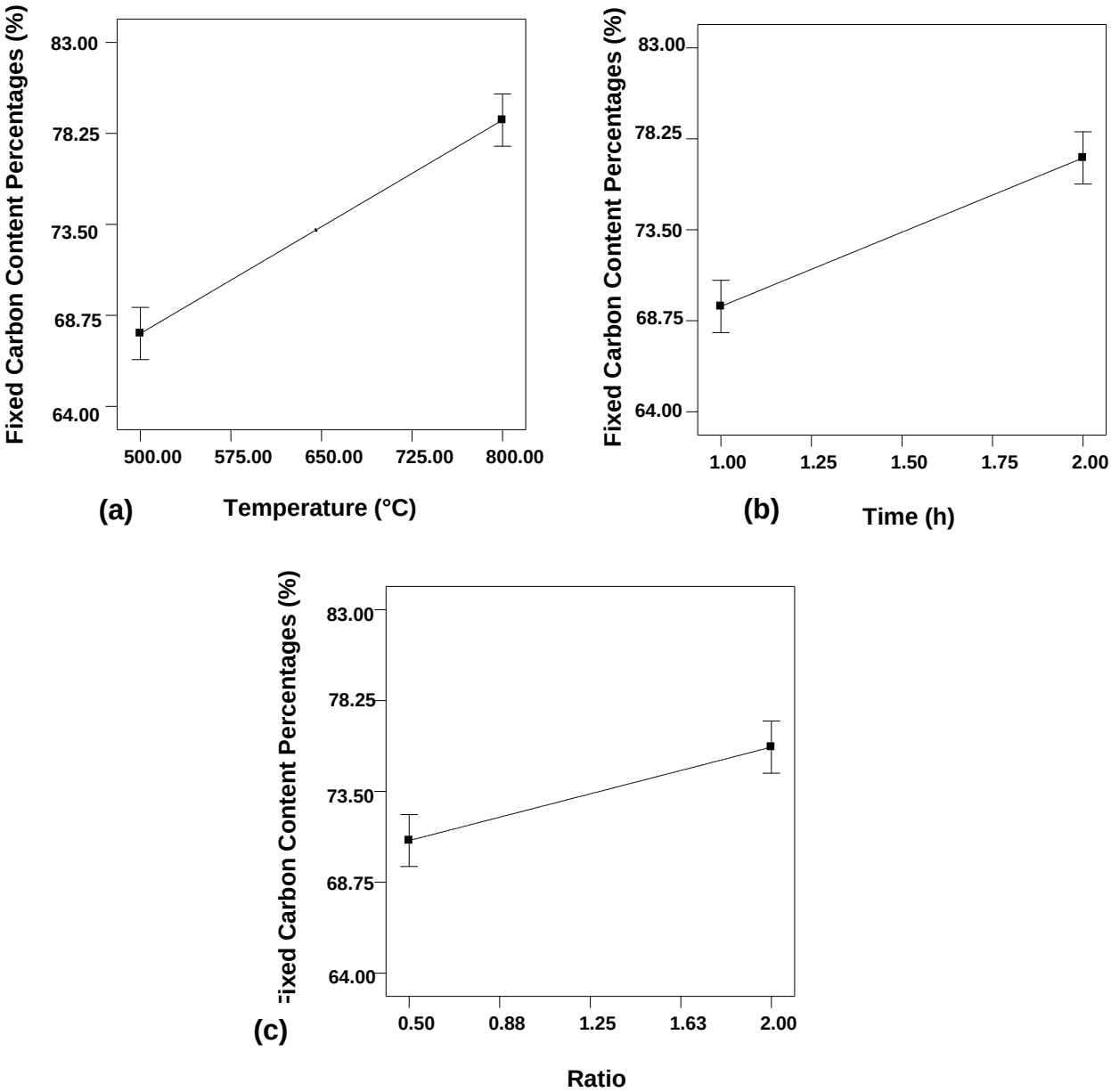

Fig. 4. Linear plots for percentage fixed carbon (β_3): (a) influence of temperature (A_1) when time (B_1) was 1.5 h and ratio (C_1) was constant at zero/center point 1.25; (b) influence of time (B_1) when ratio (C_1) was 1.25 and temperature (A_1) was constant at zero/center point 650 °C; (c) influence of ratio (C_1) when temperature (A_1) was 650 °C and time (B_1) was constant at zero/center points 1.5 h

The impact of processing variables on fixed carbon percentages (β_3)

The effect of reaction temperature (A_1) and pyrolysis time (B_1) on fixed carbon percentages (β_3) is represented in Fig. 4(a), where ratio (C_1) was kept at zero/center level. The influence of pyrolysis time (B_1) and impregnation ratio (C_1) on activated carbon yield (β_2) percentages are shown by Fig. 4(b). The influence of impregnation ratio (C_1) and temperature (A_1) is shown by Fig. 4(c).

A linear model was proposed for fixed carbon content percentages (β_3). Relatively higher temperature initiates to have more fixed carbon proportion inside the samples. At higher temperature, volatilization of organic compounds took place completely, leaving behind pure activated carbon. The ratio of K_2CO_3 also had significant impact on fixed carbon development. Fixed carbon content was increasing with increasing temperature. All three input variables had a positive impact on fixed carbon content percentages (β_3). Increasing temperature (A_1), time (B_1), and ratio (C_1) increased the percentage fixed carbon content (β_3) of the sample. Temperature (A_1) had the major influence on fixed carbon content (β_3), with a maximum F value of 37.23 (Table 5). In contrast, time (B_1) had a relatively less significant effect (F value of 43.44). With increasing temperature (A_1), duration (B_1), and ratio (C_1), K_2CO_3 can diffuse more inside the hydrochar matrix to enhance the fixed carbon content (β_3). A similar phenomenon was reported for microwave-induced KOH and NaOH activation process, preparing ACs from orange peel (Lam *et al.* 2017).

Process optimization

The optimization technique employed in this study was a numerical technique that is based on error analysis between experimental and predicted results obtained from the software. To conduct the optimization process, a maximization target was chosen for each response. The settings for the input variables were chosen within the studied range. The results obtained after the numerical optimization are provided in Table 6. Under the optimum conditions as suggested in Table-6, BSPC was activated to produce optimum BSPAC sample. The predicted and experimental values obtained for all three responses showed minimum error percentages. Hence, the models developed here were valid and can effectively illustrate the relationship between the input and output variables (Al-mahbashi *et al.* 2023).

Table 6. Preparation Conditions Optimization for BSPAC

Temp.	Time	Ratio	Percentage Removal (β_1)			Yield Percentages (β_2)			Fixed Carbon Content (β_3)		
(°C)	(h)		Pre.	Exp.	Error	Pre.	Exp.	Error	Pre.	Exp.	Error
720.48	1.80	1.17	79.50	78.51	1.24	83.22	80.02	3.84	78.48	80.90	3.08

Chracterizations

Figure 5 (a through c) shows FESEM images of raw BSP, BSPC, and BSPAC produced under optimum activation conditions using CO_2 gas flow. As illustrated in Fig. 8(a), the untreated biomass feedstock of BSP had non-porous texture with a rather uniform surface with minimal amount of cracking, cavities, or pores. The BSP had a comparatively smoother external surface, with occasional fragments of particles deposited over it (Fig. 8a).

Seed or wood type starting biomass is mainly composed of cellulose, hemicellulose, and lignin, with trace amounts of wax and pectin. Lignin and hemicellulose assist to bundle the long cellulosic threads, which results in a homogeneous surface with reduced deformation and cracking in BSP, as illustrated in Fig. 5(a). The surface of BSPC became rough enough after hydrothermal carbonization (HTC), where water act as green catalyst to produce H^+ and OH^- ions at high pressure to rupture the surface and dissolve some proportions of lignin, resulting some hollow spaces and cracks (Fig. 8b). Some small fragments of particles were clogging the pores, which could be attributed to the fractional breakdown of lignin and hemicellulose. Prior to the semi-carbonization process under HTC process, it was practically non-porous. The HTC procedure, conducted under aqueous conditions, led to the generation of a limited number of pores and cracks on the surface of BSPC (Fig. 5b).

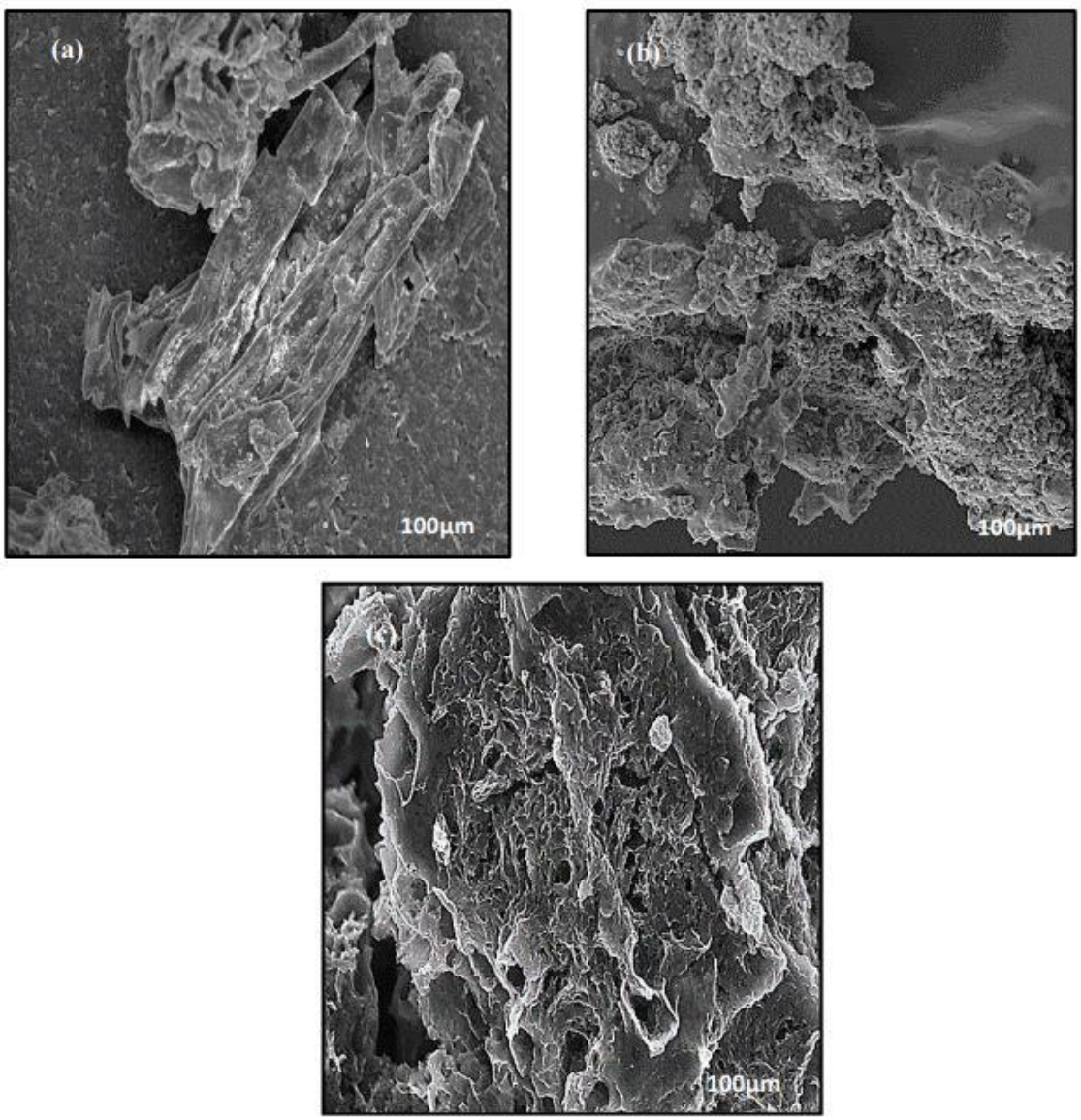

Fig. 5. FESEM Images of (a) BSP; (b) BSPC; and (c) BSPAC

During the fixed bed pyrolysis process, the addition of K_2CO_3 impregnated hydrochar with CO_2 gas flow had led to the formation of many pores with uneven shapes, as depicted in Fig. 5c. The reducing property of carbon can initiate to form K, K_2O, CO, and CO_2 gas from K_2CO_3 as represented by following equations (Sellamuthu *et al.* 2023):

$$K_2CO_3 \longrightarrow K_2O + CO_2$$
$$K_2CO_3 + 2C \longrightarrow 2K + 3CO$$
$$K_2O + 2C \longrightarrow 2K + CO$$

Metallic potassium (K) generated during the pyrolysis is anticipated to infiltrate into the inner surfaces of the hydrochar (BSPC), widening pre-existing gaps and cavities, which can aid in developing new pores (Chowdhury *et al.* 2015). The diameter of the pores can be controlled by the surface reactions as well as the amount and the quantity of volatile chemicals released. Furthermore, the dimension and structure of the pores are strongly reliant on not only the magnitude of the activation period, temperature, the ratio, the design of the reactor, rate, and type of gas flow, as well as initial pretreatment type and the catalyst used for char formation. The surface morphology after the chemical pyrolysis process was changed drastically (Fig. 5c). As a result of the fixed bed pyrolysis procedure, the pore volume with surface area dramatically increased. The BET analysis of the BSPC and BSPAC samples provides additional evidence for this phenomenon.

Thermal stability of raw, untreated biomass of BSP, its respective hydrochar BSPC, as well as the corresponding Acs namely BSPAC were determined by thermogravimetric (TGA) analysis. The percentage of fixed carbon is a crucial factor in the sorption process. It is apparent that samples with higher fixed carbon content exhibit greater removal efficiency and contain the least amount of impurities such as ash.

The BSPAC exhibited superior thermal stability in comparison to BSPC and BSP. The dtg_{max} values for BSP, BSPC, and BSPAC were 357.5, 372.3, and 386 °C, respectively, as shown in Table 6. Hemicellulose, content of LCB wastes, has relatively lower thermal stability compared to the other components (cellulose and lignin). The BSP sample underwent a process of partial carbonization using hydrothermal treatment (HTC), followed by fixed bed pyrolysis. The amorphous region of cellulose and hemicellulose will be removed during HTC and pyrolysis process. Thus, the BSPAC exhibited a greater proportion of stabilized carbon fragments that had greater resistance to high temperatures.

The first phase of degradation, occurring between 70 ℃ and 130 °C, is ascribed to the evaporation of water. For LCB wastes, the second stage of decomposition happens within the temperature range of 200 to 300 °C. This temperature range is associated with the destruction of hemicellulose, present inside the LCB matrix. Cellulose undergoes degradation within the temperature range of 300 to 400 ºC. Hemicellulose and cellulose breakdown occur simultaneously. Nevertheless, it has been observed that the degradation of lignin occurs within the temperature range of 200 to 800 °C (Chowdhury *et al.* 2015; Liu and Guo 2015). Through hydrothermal pre-treatment (HTC) or semi-carbonization, and chemical activation using fixed bed pyrolysis, the carbon content of BSP was enhanced from 50.6% to 80.9% (Table 7).

Table 8 provides the results of the ultimate analysis of raw precursors or untreated biomass of BSP, its respective hydrochar of BSPC, and their corresponding ACs, namely BSPAC. After semi-carbonization under HTC environment and fixed bed pyrolysis using K_2CO_3, the percentage carbon in the BSPC and BSPAC samples were increased. The proportions of oxygen and hydrogen contents decreased (Liu and Guo 2015). This is

because hydrothermal carbonization, often referred to as semi-carbonization and chemical pyrolysis, stimulate the disintegration of volatile compounds and the degradation of organic molecules, resulting in a very pure and robust form of carbon. Both the H/C and O/C ratios declined because of pre-treatment of BSP under HTC process and pyrolysis for activation (Liu and Guo 2015). Due to the aromatization mechanism, the H/C ratio tends to decrease during the HTC process. Additionally, the O/C ratio decreases because of the decarboxylation reactions. Dehydration can also decrease the O/C and H/C ratios.

Table 7. Thermogravimetric- (Proximate-TGA) Analysis of Starting Precursors or Lignocellulosic Residues (LCB) of BSP with its Respective Hydrochar (BSPC) and Activated Samples (BSPAC)Proximate Analysis (TGA)

Sample	**BSP**	**BSPC**	**BSPAC**
Carbon Content (%)	50.62	72.75	80.90
Moisture (%)	4.88	3.77	1.36
Volatile Matter (%)	35.28	11.53	2.59
Ash Residues (%)	9.22	11.55	14.13
dtg_{max}	357.48	372.34	385.67

Table 8. Ultimate Analysis of Starting Precursors or Lignocellulosic Residues (LCB) with their Respective Hydrochar (BSPC) and Activated Samples (BSPAC)

Ultimate Analysis	**BSP**	**BSPC**	**BSPAC**
Carbon (%)	52.87	75.01	81.90
Hydrogen (%)	9.87	5.05	3.55
Nitrogen (%)	0.68	0.64	0.35
Oxygen (%)	35.37	18.22	13.88
Others (%)	1.21	1.08	0.32
H/C	0.18	0.06	0.043
O/C	0.66	0.24	0.169

The BET isotherm for surface area analysis provides basic information regarding the pore size distribution and sorption capacity of an adsorbent materials. The volume of pores and BET surface area of the hydrochar of BSPC and activated sample BSPAC are reported in Table 9. It was found that micropores account for approximately 60.1% of the total volume of BSPAC pores. The BET surface area of BSPC was increased drastically after activation and increased from 60 to 599 m^2/gm for BSPAC. Not only BET surface area, total pore volume, Langmuir surface area, pore diameter, and volume of micropores were also increased after the activation of BSPC to yield superior quality BSPAC.

Adsorption equilibrium studies

According to the fundamental theory of Langmuir model, the adsorption energy remains constant regardless of the loading on the surface, thereby exhibiting a self-determining nature. The observation suggests that the adsorption process occurred in the

absence of any interaction between the pollutant molecules and forms a monolayer of pollutants (Haq *et al.* 2021; Ghaedi *et al.* 2022;). The linear plot of C_e/q_e *versus* C_e of Cu(II) cations adsorption onto BSPAC sample was provided from where the slope showed the values of $1/q_{max}$ (Fig. 6a) at 30 °C. The intercept of the linear line is showing the values of $1/q_{max}K_L$; from where-the values of Langmuir constant K_L was determined (Fig. 6a).

Table 9. Surface Textural Properties (Surface Area and Pore size Distribution)

Analysis/ Sample	S_{BET} (m^2/g)	S_{mic} (m^2/g)	Lang-muir Surf. Area (m^2/g)	Ext. Surf. Area (m^2/g)	S_{mic}/S_{BET} (%)	V_{mic} (cm^3/g)	V_{tot} (cm^3/g)	Diameter (nm)	Removal % of Cu(II) Cations
BSPC	60.0	75.8	800	249	0.79	0.078	0.190	1.06	59.3
BSPAC	599	500	1032	692	0.83	0.592	0.986	6.25	78.5

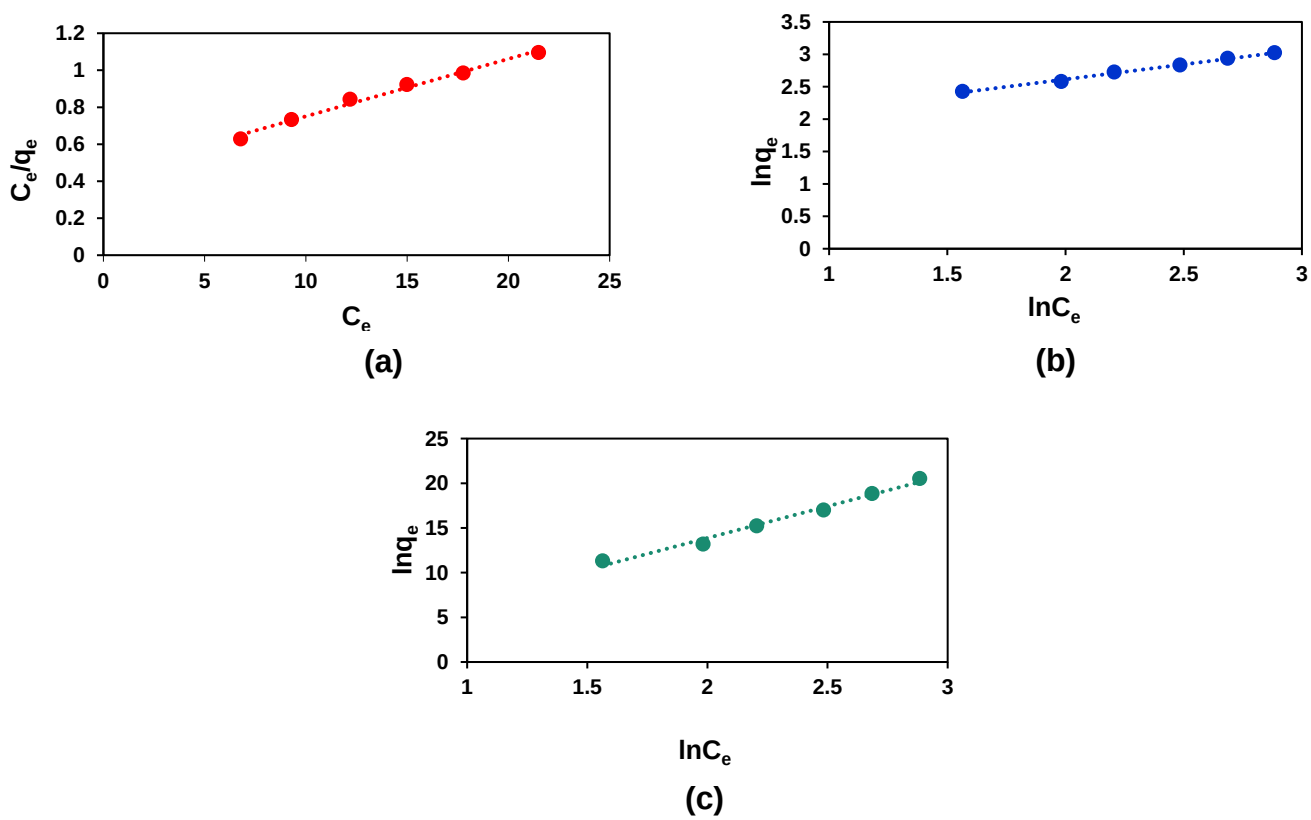

Fig. 6. Linear regression isotherm plots for (a) Langmuir; (b) Freundlich; and (c) Temkin Isotherm at 30 °C for all the studied concentration ranges with at pH 5.5 and agitation speed of 250 rpm for BSPAC

The Freundlich plots of $\ln C_e$ *versus* $\ln q_e$ gave a straight line where the values of $1/n$ are provided by slope and $\ln K_F$ was obtained from intercept. The value of $1/n$ provides the information regarding the favourable or unfavourable process, whereas K_F (mg/g (L/mg)*1/n*) indicates the intensity of the adsorption process (Fig. 6b) (Ghaedi *et al.* 2022).

According to the Temkin isotherm, the heat of adsorption for a pollutant adsorbate tends to diminish linearly as it approaches maximum surface coverage, a phenomenon

linked to the interactions between the pollutant and the adsorbent surface. The linear plot of lnC_e *versus* q_e for BSPAC at 30 °C temperature is illustrated in Fig. 6c.

At different temperature, isotherm model parameters were estimated and listed in Table 10. The Freundlich constant *1/n* determined were below 1.0 for all the temperature range studied here. Similar phenomenon was reported earlier for adsorption of copper (II) cations using modified shrimp materials (Rahman 2024). Freundlich affinity factor, K_F was decreasing with increasing temperature. The values of R_L obtained from Langmuir isotherm were below 1.0, reflecting favourable sorption process (Hamid *et al.* 2014). Langmuir monolayer adsorption capacity, q_m (mg/g) increased from 30 to 50 °C. After that, at 70 °C it was decreased to 35.5 mg/g. The values of *1/n* below 1.0 reflected that, the surface of BSPAC was heterogenous and the process was favourable here (Hamid *et al.* 2014). Recently modified shrimp was used as adsorbent for removal of Cu(II) cations, where Langmuir monolayer adsorption capacity, q_{max} (mg/g) was obtained to 20.2 mg/g, which was lower than the value obtained (32.2 mg/g) here (Rahman 2024).

Table 10. Langmuir, Freundlich, and Temkin Model Parameters at Different Temperature using BSPAC

Isotherm Model	Temperature (°C)	Maximum Monolayer Adsorption Capacity q_{max} (mg/g)	Langmuir Constant K_L (l/mg)	Separation Factor R_L	Correlation Coefficient R^2
Langmuir	30	32.25	0.0703	0.1244	0.9887
	50	41.66	0.0384	0.2063	0.9705
	70	35.46	0.0396	0.2015	0.9993
Freundlich	Temperature (°C)	Affinity Factor/Constant K_F (mg/g(L/mg)1/n)		Freundlich Exponents 1/*n*	Correlation Coefficient R^2
	30	5.4335		0.4608	0.9956
	50	2.5792		0.6520	0.9846
	70	2.5375		0.6050	0.9974
Temkin	Temperature (°C)	Binding Constant K_T (l/g)		Temkin Constant *B*	Correlation Coefficient R^2
	30	0.9550		7.1009	0.9859
	50	0.3421		9.4123	0.9918
	70	0.3297		8.3401	0.9982

CONCLUSIONS

1. In this work, baobab seed powder (BSP) was carbonized to generate BSPC hydrochar. This had a lower surface area, so it was less effective at removing Cu(II) cations from wastewater (59.3%).
2. The BSPC was further activated to achieve a higher removal efficiency of 86.4% from a concentration of 50 mg/L. Nevertheless, when the concentration was increased, a

significant 78.5% of Cu(II) cations were eliminated from a solution with an initial concentration of 100 mg/L.

3. The activation process was statistically optimized, and relevant mathematical models were developed based on response surface technique using Box Behnken design. Under optimum conditions, activation process was carried out and statistical error between predicted and experimental results obtained for removal percentages (β_1), yield (β_2), and fixed carbon content (β_3) were evaluated. The error percentages observed for percentage removal (β_1), yield (β_2), and fixed carbon content (β_3) were 1.24%, 3.84%, and 3.08%, respectively.
4. Synthesized BSPAC samples were used to remove Cu(II) cations from wastewater. The system reached equilibrium around 120 min. After that, no significant amount of adsorption took place.
5. With increasing initial concentration and contact time, BSPAC showed better equilibrium sorption capacity, q_e(mg/g). Removal percentages decreased with increasing initial concentration.
6. The magnitude of Freundlich parameter 1/n as well as Langmuir separation factor R_L obtained were below 1.0, reflecting favorable sorption process.

After being pretreated using the hydrothermal carbonization (HTC) method, the lignocellulosic waste recycled from BSP showed improved capacity to remove Cu(II) cations from effluent through chemical activation.

ACKNOWLEDGMENTS

The authors are thankful for the funding provided by ST-077-2022, M.G. 025-2022, and IIRG003A-2022IISS under the Principal Investigator Dr. Zaira Zaman Chowdhury of University of Malaya, Kuala Lumpur 50603, Malaysia. The authors extend their appreciation to the Deanship of Scientific Research at the King Khalid University for funding this work through the large Group of Project under grant number RGP:2/201/44.

REFERENCES CITED

Abbas, A. F., and Ahmed, M. J. (2016). "Mesoporous activated carbon from date stones (*Phoenix dactylifera* L.) by one-step microwave assisted K_2CO_3 pyrolysis," *Journal of Water Process Engineering* 9, 201-207. DOI: 10.1016/j.jwpe.2016.01.004

Adebisi, G. A., Chowdhury, Z. Z., and Alba, P. A. (2017a). "Equilibrium, kinetic, and thermodynamic studies of lead ion and zinc ion adsorption from aqueous solution onto activated carbon prepared from palm oil mill effluent," *Journal of Cleaner Production* 148, 958-968. DOI: 10.1016/j.jclepro.2017.02.047

Adebisi, G. A., Chowdhury, Z. Z., Hamid, S. B. A., and Ali, E. (2017b). "Equilibrium isotherm, kinetic, and thermodynamic studies of divalent cation adsorption onto *Calamus gracilis* sawdust-based activated carbon," *BioResources* 12(2), 2872-2898. DOI: 10.15376/biores.12.2.2872-2898

Adebisi, G. A., Chowdhury, Z. Z., Abd Hamid, S. B., and Ali, E. (2016). "Hydrothermally treated banana empty fruit bunch fiber activated carbon for Pb(II)

and Zn(II) removal," *BioResources* 11(4), 9686-9709. DOI: 10.15376/biores.11.4.9686-9709

Ahmad, M. A., Ahmad Puad, N. A., and Bello, O. S. (2014). "Kinetic, equilibrium and thermodynamic studies of synthetic dye removal using pomegranate peel activated carbon prepared by microwave-induced KOH activation," *Water Resources and Industry* 6, 18-35. DOI: 10.1016/j.wri.2014.06.002

Alcaraz, L., García-Díaz, I., Alguacil, F. J., and Lopez, F. A. (2020). "Removal of copper ions from wastewater by adsorption onto a green adsorbent from winemaking wastes," *BioResources* 15(1), 1112-1133. DOI: 10:10.15376/biores.15.1.1112-1133

Ali, A. E., Chowdhury, Z. Z., Devnath, R., Ahmed, M. M., Rahman, M. M., Khalid, K., Wahab, Y. A., Badruddin, I. A., Kamangar, S., Hussien, M., *et al.* (2023). "Removal of Azo dyes from aqueous effluent using bio-based activated carbons: Toxicity aspects and environmental impact," *Separations* 10(9), article 506. DOI: 10.3390/separations10090506.

Ali, Z., Khan, I., Iqbal, M. S., Zhang, Q., Ai, X., Shi, H., Ding, L., and Hong, M. (2023). "Toxicological effects of copper on bioaccumulation and mRNA expression of antioxidant, immune, and apoptosis-related genes in Chinese, striped-necked turtle (*Mauremys sinensis*)," *Frontiers in Physiology* 14, article 1296259. DOI: 10.3389/fphys.2023.1296259

Al-mahbashi, N. M. Y., Kutty, S., Jagaba, A., Al-nini, A., Sholagberu, A. T., Aldhawi, B. N., and Rathnayake, U. (2023). "Sustainable sewage sludge biosorbent activated carbon for remediation of heavy metals: Optimization by response surface methodology," *Case Studies in Chemical and Environmental Engineering* 8, article ID 100437. DOI: 10.1016/j.cscee.2023.100437

Akinpelu, A. A., Chowdhury, Z. Z., Shibly, S. M., Faisal, A. N., Badruddin, I. A., Rahman, M. M., Amin, M. A., Sagadevan, S., Akbarzadeh, O., Khan, T. M., *et al.* (2021). "Adsorption studies of volatile organic compound (Naphthalene) from aqueous effluents: Chemical activation process using weak Lewis acid, equilibrium kinetics and isotherm modelling," *International Journal of Molecular Sciences* 22(4), article 2090. DOI: 10.3390/ijms22042090

Ayed, L., Bouguerra, A., Charef, A., Bakhrouf, A., and Mzoughi, R. E. (2019). "Biodegradation of olive mill wastewater by a newly isolated novel bacterial consortium under RSM optimized culture conditions," *Journal of Water Process Engineering* 32, article ID 100986. DOI: 10.1016/j.jwpe.2019.100986

Benavente, V., Calabuig, E., and Fullana, A. (2015). "Upgrading of moist agro-industrial wastes by hydrothermal carbonization," *Journal of Analytical and Applied Pyrolysis* 113, 89-98. DOI: 10.1016/j.jaap.2014.11.004

Chowdhury, Z. Z., Zain, S. M., Khan, R. A., Arami-Niya, A., and Khalid, K. (2012). "Process variables optimization for preparation and characterization of novel adsorbent from lignocellulosic waste," *BioResources* 7(3), 3732-3754. DOI: 10.5736/biores.7.3.3732-3754

Chowdhury, Z. Z., Hasan, M. R., Abd Hamid, S. B., Samsudin, E. M., Zain, S. M., and Khalid, K. (2015). "Catalytic pretreatment of biochar residues derived from lignocellulosic feedstock for equilibrium studies of manganese, Mn(II) cations from aqueous solution," *RSC Advances* 5, 6345-6356. DOI: 10.1039/C4RA09709B

Chowdhury, Z. Z., Yehye, W. A., Julkapli, N. M., Al Saadi, M. A. H., and Atieh, M. A. (2016a). "Application of graphitic bio-carbon using two-level factorial design for

microwave-assisted carbonization," *BioResources* 11(2), 3637-3659. DOI: 10.15376/biores.11.2.3637-3659

Chowdhury, Z. Z., Abd Hamid, S. B., Rahman, M. M., and Rafique, R. F. (2016b). "Catalytic activation and application of micro-spherical carbon derived from hydrothermal carbonization of lignocellulosic biomass: Statistical analysis using Box–Behnken design," *RSC Advances* 6(104), 102680-102694. DOI: 10.1039/C5RA26189A

Chowdhury, Z. Z., Karim, M. Z., Ashraf, M. A., and Khalid, K. (2016c). "Influence of carbonization temperature on physicochemical properties of biochar derived from slow pyrolysis of durian wood (*Durio zibethinus*) sawdust," *BioResources* 11(2), 3356-3372. DOI: 10.15376/biores.11.2.3356-3372

Chowdhury, Z. Z., Pal, K., Johan, R. B., Dabdawb, W. A., Ali, M. E., and Rafique, R. F. (2017). "Comparative evaluation of physiochemical properties of a solid fuel derived from *Adansonia digitata* trunk using torrefaction," *BioResources* 12(2), 3816-3833. DOI: 10.15376/BIORES.12.2.3816-3833

Chowdhury, Z. Z., Krishnan, B., Sagadevan, S., Rafique, R. F., Hamizi, N. A., Abdul Wahab, Y., Khan, A. A., Johan, R. B., Kazi, S. N., and Tawab Shah, S. (2018). "Effect of temperature on the physical, electro-chemical and adsorption properties of carbon micro-spheres using hydrothermal carbonization process," *Nanomaterials* 8(8), article 597. DOI: 10.3390/nano8080597

Doan, V. D., Tran, T. K., Nguyen, A., Tran, V. A., Nguyen, T. D., and Le, V. T. (2021). "Comparative study on adsorption of cationic and anionic dyes by nanomagnetite supported on biochar derived from *Eichhornia crassipes* and *Phragmites australis* stems," *Environmental Nanotechnology, Monitoring & Management* 16, article ID 100569. DOI: 10.1016/j.enmm.2021.100569

Ferrera-Lorenzo, N., Fuente, E., Suárez-Ruiz, I., and Ruiz, B. (2014). "KOH activated carbon from conventional and microwave heating system of a macroalgae waste from the Agar–Agar industry," *Fuel Processing Technology* 121, 25-31. DOI: 10.1016/j.fuproc.2013.12.017

Fierro, V., Muñiz, G., Basta, A. H., El-Saied, H., and Celzard, A. (2010). "Rice straw as precursor of activated carbons: activation with ortho-phosphoric acid," *Journal of Hazardous Materials* 181(1-3), 27-34. DOI: 10.1016/j.jhazmat.2010.04.062

Foo, K., Lee, L., and Hameed, B. (2013). "Preparation of banana frond activated carbon by microwave induced activation for the removal of boron and total iron from landfill leachate," *Chemical Engineering Journal* 223, 604-610. DOI: 10.1016/j.cej.2013.03.009

Ghaedi, S., Seifpanahi-Shabani, K., and Sillanpää, M. (2022). "Waste-to-resource: New application of modified mine silicate waste to remove Pb^{2+} ion and methylene blue dye, adsorption properties, mechanism of action and recycling," *Chemosphere* 292, article ID 133412. DOI: 10.1016/j.chemosphere.2021.133412

Hamid, S. B. A., Chowdhury, Z. Z., and Zain, S. M. (2014). "Base catalytic approach: A promising technique for the activation of biochar for equilibrium sorption studies of Copper, Cu(II) ions in single solute system," *Materials 7*(4), 2815-2832. DOI: 10.3390/ma7042815

Haq, A. U., Saeed, M., Usman, M., Zahoor, A. F., Anjum, M. N., Maqbool, T., Naheed, S., and Kashif, M. (2021). "Mechanisms of halosulfuron methyl pesticide biosorption onto neem seeds powder," *Scientific Reports* 11(1), article Number 9960. DOI: 10.1038/s41598-021-88929-7

Ho, C., Yu, J., Yang, S., Ya, V., Le, H. A., Cheng, L., Choo, K., and Li, C. (2021). "Use of packed scrap iron anodes for continuous electrochemical Cr(VI) reduction process in electroplating wastewater treatment," *Journal of Water Process Engineering* 42, article ID 102191. DOI: 10.1016/j.jwpe.2021.102191

Huang, Y., and Garcia-Bennett, A. E. (2021). "Equilibrium and kinetic study of l- and d-valine adsorption in supramolecular-templated chiral mesoporous materials," *Molecules* 26(2), article 338. DOI: 10.3390/molecules26020338

Jiang, Y., Liu, C., and Huang, A. (2019). "EDTA-functionalized covalent organic framework for the removal of heavy-metal ions," *ACS Applied Materials & Interfaces* 11, 32186-32191. DOI: 10.1021/acsami.9b11850

Jin, J., Li, S., Peng, X., Liu, W., Zhang, C., Yang, Y., Han, L., Du, Z., Sun, K., and Wang, X. (2018). "HNO_3 modified biochars for uranium (VI) removal from aqueous solution," *Bioresource Technology* 256, 247-253. DOI: 10.1016/j.biortech.2018.02.022

Kundu, A., Sen Gupta, B., Hashim, M., and Redzwan, G. (2015). "Taguchi optimization approach for production of activated carbon from phosphoric acid impregnated palm kernel shell by microwave heating," *Journal of Cleaner Production* 105, 420-427. DOI: 10.1016/j.jclepro.2014.06.093

Lam, S. S., Liew, R. K., Wong, Y. M., Yek, P. N. Y., Ma, N. L., Lee, C. L., and Chase, H. A. (2017). "Microwave-assisted pyrolysis with chemical activation, an innovative method to convert orange peel into activated carbon with improved properties as dye adsorbent," *Journal of Cleaner Production* 162, 1376-1387. DOI: 10.1016/j.jclepro.2017.06.131

Liu, F. J., and Guo, M. (2015). "Comparison of the characteristics of hydrothermal carbons derived from holocellulose and crude biomass," *Journal of Materials Science* 50, 1624-1631. DOI: 10.1007/s10853-014-8723-0

Maldhure, A. V., and Ekhe, J. (2011). "Preparation and characterizations of microwave assisted activated carbons from industrial waste lignin for Cu(II) sorption," *Chemical Engineering Journal* 168(3), 1103-1111. DOI: 10.1016/j.cej.2011.01.091

Mittal, H., Al Alili, A., Morajkar, P. P., and Alhassan, S. M. (2021). "Graphene oxide crosslinked hydrogel nanocomposites of xanthan gum for the adsorption of crystal violet dye," *Journal of Molecular Liquids* 323, article ID 115034. DOI: 10.1016/j.molliq.2020.115034

Mulungulungu, G. A., Mao, T., and Han, K. (2021). "Efficient removal of high-concentration copper ions from wastewater *via* 2D g-C_3N_4 photocatalytic membrane filtration," *Colloids and Surfaces A: Physicochemical and Engineering Aspects* 623, article ID 126714. DOI: 10.1016/j.colsurfa.2021.126714

Namazi, A. B., Grant Allen, D., and Jia, C. Q. (2015). "Microwave-assisted pyrolysis and activation of pulp mill sludge," *Biomass and Bioenergy* 73, 217-224. DOI: 10.1016/j.biombioe.2014.12.023

Njoku, V., Foo, K., Asif, M., and Hameed, B. (2014). "Preparation of activated carbons from rambutan (*Nephelium lappaceum*) peel by microwave-induced KOH activation for acid yellow 17 dye adsorption," *Chemical Engineering Journal* 250, 198-204. DOI: 10.1016/j.cej.2014.03.115

Patel, A., and Shah, A. R. (2021). "Integrated lignocellulosic biorefinery: Gateway for production of second-generation ethanol and value-added products," *Journal of Bioresources and Bioproducts* 6(2), 108-128. DOI: 10.1016/j.jobab.2021.02.001

Pezoti Junior, O., Cazetta, A. L., Gomes, R. C., Barizão, É. O., Souza, I. P., Martins, A. C., Asefa, T., and Almeida, V. C. (2013). "Synthesis of $ZnCl_2$-activated carbon from macadamia nut endocarp (*Macadamia integrifolia*) by microwave-assisted pyrolysis: Optimization using RSM and methylene blue adsorption," *Journal of Analytical and Applied Pyrolysis* 105, 166-176. DOI: 10.1016/j.jaap.2013.10.015

Rahman, A. (2024). "Promising and environmentally friendly removal of copper, zinc, cadmium, and lead from wastewater using modified shrimp-based chitosan," *Water* 16(1), article 184. DOI: 10.3390/w16010184

Rajesh Banu, J., Kavitha, S., Tyagi, V. K., Gunasekaran, M., Karthikeyan, O. P., and Kumar, G. (2021). "Lignocellulosic biomass based biorefinery: A successful platform towards circular bioeconomy," *Fuel* 302, article ID 121086. DOI: 10.1016/j.fuel.2021.121086

Rego, R. M., Sriram, G., Ajeya, K. V., Jung, H. Y., Kurkuri, M. D., and Kigga, M. (2021). "Cerium based UiO-66 MOF as a multipollutant adsorbent for universal water purification," *Journal of hazardous materials* 416, article ID 125941. DOI: 10.1016/j.jhazmat.2021.125941

Saucier, C., Adebayo, M. A., Lima, E. C., Cataluña, R., Thue, P. S., Prola, L. D. T., Puchana-Rosero, M. J., Machado, F. M., Pavan, F. A., and Dotto, G. L. (2015). "Microwave-assisted activated carbon from cocoa shell as adsorbent for removal of sodium diclofenac and nimesulide from aqueous effluents," *Journal of Hazardous Materials* 289, 18-27. DOI: 10.1016/j.jhazmat.2015.02.026

Sellamuthu, S., Chowdhury, Z. Z., Khalid, K., Shibly, S. M., Rahman, M. M., Rana, M., Badruddin, I. A., Khaleed, H. M., Kamangar, S., Johan, M. R., *et al.* (2023). "Mathematical modelling and optimization for facile synthesis of structured activated carbon (ACs) from *Adansonia kilima (Baobab)* wood chips integrating microwave-assisted pyrolysis for the elimination of lead (II) cations from wastewater effluents," *Molecules* 28(18), article ID 6640. DOI: 10.3390/molecules28186640

Singh, N., Singhania, R. R., Nigam, P. S., Dong, C. D., Patel, A. K., and Puri, M. (2022). "Global status of lignocellulosic biorefinery: Challenges and perspectives," *Bioresource Technology* 344(Part B), article ID 126415. DOI: 10.1016/j.biortech.2021.126415

Tsai, T., Chou, H., and Wu, Y. (2020). "Removal of nickel from chemical plating waste solution through precipitation and production of microsized nickel hydroxide particles," *Separation and Purification Technology* 251, article ID 117315. DOI: 10.1016/j.seppur.2020.117315

Virolainen, S., Wesselborg, T., Kaukinen, A., and Sainio, T. (2021). "Removal of iron, aluminium, manganese and copper from leach solutions of lithium-ion battery waste using ion exchange," *Hydrometallurgy* 202, article ID 105602. DOI: 10.1016/j.hydromet.2021.105602

Wang, Y.-H., and Wu, J.-J. (2023). "Thermochemical conversion of biomass: Potential future prospects," *Renewable and Sustainable Energy Reviews* 187, article 113754, DOI: 10.1016/j.rser.2023.113754.

Yu, B., Liu, X., Ji, C., and Sun, H. (2023). "Greenhouse gas mitigation strategies and decision support for the utilization of agricultural waste systems: A case study of Jiangxi Province, China," *Energy* 265, article ID 126380. DOI: 10.1016/j.energy.2022.126380

Zheng, Z., Xia, H., Srinivasakannan, C., Peng, J., and Zhang, L. (2014). "Utilization of Crofton weed for preparation of activated carbon by microwave induced CO_2

activation," *Chemical Engineering and Processing: Process Intensification* 82, 1-8. DOI: 10.1016/j.cep.2014.05.001

Zhu, L., Lei, H., Wang, L., Yadavalli, G., Zhang, X., Wei, Y., Liu, Y., Yan, D., Chen, S., and Ahring, B. (2015). "Biochar of corn stover: Microwave-assisted pyrolysis condition induced changes in surface functional groups and characteristics," *Journal of Analytical and Applied Pyrolysis* 115, 149-156. DOI: 10.1016/j.jaap.2015.07.012

Article submitted: December 20, 2023; Peer review completed: February 11, 2024; Revised version received: March 8, 2024; Accepted: March 9, 2024; Published: April 25, 2024.
DOI: 10.15376/biores.19.2.3699-3724